Electromagnetic signatures of thin accretion disks in wormhole geometries

Tiberiu Harko*
Department of Physics and Center for Theoretical and Computational Physics, The University of Hong Kong, Pok Fu Lam Road, Hong Kong

Zoltán Kovács†
Max-Planck-Institute für Radioastronomie, Auf dem Hügel 69, 53121 Bonn, Germany and Department of Experimental Physics, University of Szeged, Dóm Tér 9, Szeged 6720, Hungary

Francisco S. N. Lobo‡
Institute of Cosmology & Gravitation, University of Portsmouth, Portsmouth PO1 2EG, UK and Centro de Astronomia e Astrofísica da Universidade de Lisboa, Campo Grande, Ed. C8 1749-016 Lisboa, Portugal

(Dated: September 12, 2008)

In this paper, we study the physical properties and characteristics of matter forming thin accretion disks in static and spherically symmetric wormhole spacetimes. In particular, the time averaged energy flux, the disk temperature and the emission spectra of the accretion disks are obtained for these exotic geometries, and are compared with the Schwarzschild solution. It is shown that more energy is emitted from the disk in a wormhole geometry than in the case of the Schwarzschild potential and the conversion efficiency of the accreted mass into radiation is more than a factor of two higher for the wormholes than for static black holes. These effects in the disk radiation are confirmed in the radial profiles of temperature corresponding to theses flux distributions, and in the emission spectrum $\omega L(\omega)$ of the accretion disks. We conclude that specific signatures appear in the electromagnetic spectrum, thus leading to the possibility of distinguishing wormhole geometries by using astrophysical observations of the emission spectra from accretion disks.

PACS numbers: 04.50.Kd, 04.70.Bw, 97.10.Gz

I. INTRODUCTION

Most of the astrophysical bodies grow substantially in mass via accretion. Recent observations suggest that around almost all of the active galactic nuclei (AGN's), or black hole candidates, there exist gas clouds surrounding the central compact object, together with an associated accretion disk, on a variety of scales from a tenth of a parsec to a few hundred parsecs [1]. These gas clouds, existing in either a molecular or atomic phase, are assumed to form a geometrically and optically thick torus (or warped disk), which absorbs most of the ultraviolet radiation and soft X-rays. The most powerful evidence for the existence of super massive black holes comes from the VLBI (very long baseline interferometry) imaging of molecular H_2O masers in the active galaxy NGC 4258 [2]. This imaging, produced by Doppler shift measurements assuming Keplerian motion of the masering source, has allowed a quite accurate estimation of the central mass, which has been found to be a $3.6 \times 10^7 M_{\odot}$ super massive dark object, within 0.13 parsecs. Hence, important astrophysical information can be obtained from the observation of the motion of gas streams in the gravitational field of compact objects.

The mass accretion around rotating black holes was studied in general relativity for the first time in [3]. By using an equatorial approximation to the stationary and axisymmetric spacetime of rotating black holes, steady-state thin disk models were constructed, extending the theory of non-relativistic accretion [4]. In these models hydrodynamical equilibrium is maintained by efficient cooling mechanisms via radiation transport, and the accreting matter has a Keplerian rotation. The radiation emitted by the disk surface was also studied under the assumption that black body radiation would emerge from the disk in thermodynamical equilibrium. The radiation properties of thin accretion disks were further analyzed in [5, 6], where the effects of photon capture by the hole on the spin evolution were presented as well. In these works the efficiency with which black holes convert rest mass into outgoing radiation in the accretion process was also computed. More recently, the emissivity properties of the accretion disks were investigated for exotic central objects, such as non-rotating or rotating quark, boson or fermion stars [7, 8, 9, 10]. The radiation power per unit area, the temperature of the disk and the spectrum of the emitted radiation were given, and compared with the case of a Schwarzschild black hole of an equal mass. The physical properties of matter forming a thin accretion disk in the static and spherically symmetric spacetime metric of vacuum $f(R)$ modified gravity models were also analyzed [11], and it was shown that particular signatures can appear in the electromagnetic spectrum, thus leading to the possibility of directly testing modified gravity models by

*Electronic address: harko@hkucc.hku.hk
†Electronic address: zkovacs@mpifr-bonn.mpg.de
‡Electronic address: francisco.lobo@port.ac.uk

using astrophysical observations of the emission spectra from accretion disks.

It is the purpose of the present paper to study the thin accretion disk models applied for the study of wormholes, and carry out an analysis of the properties of the radiation emerging from the surface of the disk. In classical general relativity, wormholes are supported by exotic matter, which involves a stress energy tensor that violates the null energy condition (NEC) [12]. Note that the NEC is given by $T_{\mu\nu}k^\mu k^\nu \geq 0$, where k^μ is *any* null vector. Several candidates have been proposed in the literature, amongst which we refer to the first solutions with what we now call massless phantom scalar fields [13] and (probably) the first examples of multidimensional wormhole solutions [14]; solutions in higher dimensions, for instance in Einstein-Gauss-Bonnet theory [15]; wormholes on the brane [16]; solutions in Brans-Dicke theory [17]; wormhole solutions in semi-classical gravity (see Ref. [18] and references therein); exact wormhole solutions using a more systematic geometric approach were found [19]; solutions supported by equations of state responsible for the cosmic acceleration [20]; and NEC respecting geometries were further explored in conformal Weyl gravity [21], etc (see Refs. [22, 23] for more details and [23] for a recent review). Thus, it should prove interesting to analyze the properties of an accretion disk around wormholes comprising of exotic matter. In fact, we show that specific signatures appear in the electromagnetic spectrum, thus leading to the possibility of distinguishing wormhole geometries from the Schwarzschild solution by using astrophysical observations of the emission spectra from accretion disks.

The present paper is organized as follows. In Section II, we review the formalism of the thin disk accretion onto compact objects for static and spherically symmetric spacetimes. In Section III, we analyze the basic properties of matter forming a thin accretion disk in wormhole spacetimes. We discuss and conclude our results in Section IV. Throughout this work, we use a system of units so that $c = G = \hbar = k_B = 1$, where k_B is Boltzmann's constant.

II. ELECTROMAGNETIC RADIATION PROPERTIES OF THIN ACCRETION DISKS IN GENERAL RELATIVISTIC SPACETIMES

Accretion discs are flattened astronomical objects made of rapidly rotating gas which slowly spirals onto a central gravitating body, with its gravitational energy degraded to heat. A fraction of the heat converts into radiation, which partially escapes, and cools down the accretion disc. The only information that we have about accretion disk physics comes from this radiation, when it reaches radio, optical and X-ray telescopes, allowing astronomers to analyze its electromagnetic spectrum, and its time variability. A thin accretion disk is an accretion disk such that in cylindrical coordinates (r, ϕ, z) most of the matter lies close to the radial plane. For the thin accretion disk its vertical size (defined along the z-axis) is negligible, as compared to its horizontal extension (defined along the radial direction r), i.e, the disk height H, equal to the maximum half thickness of the disk, is always much smaller than the characteristic radius R of the disk, $H \ll R$.

The thin disk is in hydrodynamical equilibrium, and the pressure gradient and a vertical entropy gradient in the accreting matter are negligible. The efficient cooling via the radiation over the disk surface prevents the disk from cumulating the heat generated by stresses and dynamical friction. In turn, this equilibrium causes the disk to stabilize its thin vertical size. The thin disk has an inner edge at the marginally stable orbit of the compact object potential, and the accreting plasma has a Keplerian motion in higher orbits.

In steady state accretion disk models, the mass accretion rate $\dot{M}_0$ is assumed to be a constant that does not change with time. The physical quantities describing the orbiting plasma are averaged over a characteristic time scale, e.g. Δt, over the azimuthal angle $\Delta\phi = 2\pi$ for a total period of the orbits, and over the height H [3, 4, 5].

The particles moving in Keplerian orbits around the compact object with a rotational velocity $\Omega = d\phi/dt$ have a specific energy $\widetilde{E}$ and a specific angular momentum $\widetilde{L}$, which, in the steady state thin disk model, depend only on the radii of the orbits. These particles, orbiting with the four-velocity u^μ, form a disk of an averaged surface density Σ, the vertically integrated average of the rest mass density ρ_0 of the plasma. The accreting matter in the disk is modelled by an anisotropic fluid source, where the density ρ_0, the energy flow vector q^μ and the stress tensor $t^{\mu\nu}$ are measured in the averaged rest-frame (the specific heat was neglected). Then, the disk structure can be characterized by the surface density of the disk [3, 5],

$$\Sigma(r) = \int_{-H}^{H} \langle \rho_0 \rangle dz, \tag{1}$$

with averaged rest mass density $\langle \rho_0 \rangle$ over Δt and 2π and the torque

$$W_\phi{}^r = \int_{-H}^{H} \langle t_\phi{}^r \rangle dz, \tag{2}$$

with the averaged component $\langle t^r_\phi \rangle$ over Δt and 2π. The time and orbital average of the energy flux vector gives the radiation flux $\mathcal{F}(r)$ over the disk surface as $\mathcal{F}(r) = \langle q^z \rangle$.

The stress-energy tensor is decomposed according to

$$T^{\mu\nu} = \rho_0 u^\mu u^\nu + 2u^{(\mu}q^{\nu)} + t^{\mu\nu}, \tag{3}$$

where $u_\mu q^\mu = 0$, $u_\mu t^{\mu\nu} = 0$. The four-vectors of the energy and angular momentum flux are defined by $-E^\mu \equiv T^\mu_\nu(\partial/\partial t)^\nu$ and $J^\mu \equiv T^\mu_\nu(\partial/\partial\phi)^\nu$, respectively. The structure equations of the thin disk can be derived

by integrating the conservation laws of the rest mass, of the energy, and of the angular momentum of the plasma [3, 5]. From the equation of the rest mass conservation, $(\rho_0 u^\mu)_{;\mu} = 0$, it follows that the time averaged rate of the accretion of the rest mass is independent of the disk radius,

$$\dot{M}_0 \equiv -2\pi r \Sigma u^r = \text{constant}. \tag{4}$$

The conservation law $E^\mu{}_\mu = 0$ of the energy has the integral form

$$[\dot{M}_0 \widetilde{E} - 2\pi r \Omega W_\phi{}^r]_{,r} = 4\pi r \mathcal{F} \widetilde{E} \ , \tag{5}$$

which states that the energy transported by the rest mass flow, $\dot{M}_0 \widetilde{E}$, and transported by the dynamical stresses in the disk, $2\pi r \Omega W_\phi{}^r$, is in balance with the energy radiated away from the surface of the disk, $4\pi r \mathcal{F} \widetilde{E}$. The law of the angular momentum conservation, $J^\mu{}_\mu = 0$, also states the balance of these three forms of the angular momentum transport,

$$[\dot{M}_0 \widetilde{L} - 2\pi r W_\phi{}^r]_{,r} = 4\pi r \mathcal{F} \widetilde{L} \ . \tag{6}$$

By eliminating $W_\phi{}^r$ from Eqs. (5) and (6), and applying the universal energy-angular momentum relation $dE = \Omega dJ$ for circular geodesic orbits in the form $\widetilde{E}_{,r} = \Omega \widetilde{L}_{,r}$, the flux $\mathcal{F}$ of the radiant energy over the disk can be expressed in terms of the specific energy, angular momentum and of the angular velocity of the black hole [3, 5],

$$\mathcal{F}(r) = -\frac{\dot{M}_0}{4\pi\sqrt{-g}} \frac{\Omega_{,r}}{(\widetilde{E} - \Omega \widetilde{L})^2} \int_{r_{ms}}^{r} (\widetilde{E} - \Omega \widetilde{L}) \widetilde{L}_{,r} dr \ . \tag{7}$$

In the derivation of the above formula the "no torque" inner boundary condition was prescribed, according to which the torque vanishes at the inner edge of the disk. Thus, we assume that the accreting matter at the marginally stable orbit r_{ms} falls freely into the central compact object, and cannot exert considerable torque on the disk. The latter assumption is valid only if no strong magnetic fields exist in the plunging region, where matter falls into the compact object.

Another important characteristics of the mass accretion process is the efficiency with which the central object converts rest mass into outgoing radiation. This quantity is defined as the ratio of the rate of the radiation energy of photons escaping from the disk surface to infinity, and the rate at which mass-energy is transported to the central compact general relativistic object, both measured at infinity [3, 5]. If all the emitted photons can escape to infinity, the efficiency is given in terms of the specific energy measured at the marginally stable orbit r_{ms},

$$\epsilon = 1 - \widetilde{E}_{ms}. \tag{8}$$

For Schwarzschild black holes the efficiency ϵ is about 6%, whether the photon capture by the black hole is considered, or not. Ignoring the capture of radiation by the hole, ϵ is found to be 42% for rapidly rotating black holes, whereas the efficiency is 40% with photon capture in the Kerr potential [6].

It is possible to define a temperature $T(r)$ of the disk, by using the definition of the flux, as $\mathcal{F}(r) = \sigma T^4(r)$, where σ is the Stefan-Boltzmann constant. Considering that the disk emits as a black body, one can use the dependence of T on $\mathcal{F}$ to calculate the luminosity $L(\omega)$ of the disk through the expression for the black body spectral distribution [8],

$$L(\omega) = 4\pi d^2 I(\omega) = \frac{4}{\pi} \cos i \omega^3 \int_{r_i}^{r_f} \frac{r dr}{\exp(\omega/T) - 1}, \tag{9}$$

where d is the distance to the source, $\omega = 2\pi\nu$, where ν is the radiation frequency, $I(\omega)$ denotes the Planck distribution function, i is the inclination of the accretion disk (defined as the angle between the line of sight and the normal to the disk), and r_i and r_f indicate the position of the inner and outer edge of the disk, respectively. In the following the inclination angle i used for the calculation of the spectra is set to $\cos i = 1$.

In order to compute the flux integral given by Eq. (7), we determine the radial dependence of the angular velocity Ω, of the specific energy $\widetilde{E}$ and of the specific angular momentum $\widetilde{L}$ of particles moving in circular orbits around general relativistic compact spheres in a static and spherically symmetric geometry given by the following line element

$$ds^2 = -e^{2\Phi(r)} dt^2 + e^{2\lambda(r)} dr^2 + r^2 (d\theta^2 + \sin^2\theta \, d\phi^2) \, . \tag{10}$$

The geodesic equations for particles orbiting in the equatorial plane of the compact object can be written as

$$e^{4\Phi} \left(\frac{dt}{d\tau}\right)^2 = \widetilde{E}^2, \quad r^4 \left(\frac{d\phi}{d\tau}\right)^2 = \widetilde{L}^2, \tag{11}$$

$$e^{4(\Phi+\lambda)} \left(\frac{dr}{d\tau}\right)^2 + V_{eff}(r) = \widetilde{E}^2, \tag{12}$$

where τ is the affine parameter, and the effective potential is given by

$$V_{eff}(r) \equiv e^{2\Phi} \left(1 + \frac{\widetilde{L}^2}{r^2}\right) \ . \tag{13}$$

From the conditions $V_{eff}(r) = 0$ and $V_{eff,\,r}(r) = 0$ we obtain

$$\widetilde{E} \ = \ \frac{e^{2\Phi}}{\sqrt{e^{2\Phi} - r^2\Omega^2}} \, , \tag{14}$$

$$\widetilde{L} \ = \ \frac{r^2\Omega}{\sqrt{e^{2\Phi} - r^2\Omega^2}} \, . \tag{15}$$

$$\Omega \ = \ \sqrt{\frac{\Phi_{,r} e^{2\Phi}}{r}} \, , \tag{16}$$

where the subscript denotes differentiation with respect to the radial coordinate. The condition $V_{eff,\,rr}(r) = 0$

provides the marginally stable orbit r_{ms} (or the innermost stable circular orbit), which can be determined for any explicit expression of the function $\Phi(r)$.

III. ELECTROMAGNETIC SIGNATURES OF ACCRETION DISKS IN WORMHOLE GEOMETRIES

Consider the static and spherically symmetric metric given by

$$ds^2 = -e^{2\Phi(r)}\,dt^2 + \frac{dr^2}{1-b(r)/r} + r^2\left(d\theta^2 + \sin^2\theta\,d\phi^2\right), \tag{17}$$

which describes a wormhole geometry with two identical, asymptotically flat regions joined together at the throat $r_0 > 0$. $\Phi(r)$ and $b(r)$ are arbitrary functions of the radial coordinate r, denoted as the redshift function and the shape function, respectively. The radial coordinate has a range that increases from a minimum value at r_0, corresponding to the wormhole throat, to ∞.

To avoid the presence of event horizons, $\Phi(r)$ is imposed to be finite throughout the coordinate range. At the throat r_0, one has $b(r_0) = r_0$, and a fundamental property is the flaring-out condition given by $(b'r - b)/b^2 < 0$, which is provided by the mathematics of embedding [12].

An interesting feature of wormhole geometries are their repulsive/attractive character [24]. To verify this, consider the four-velocity of a static observer, at rest at constant r, θ, ϕ, given by $u^\mu = dx^\mu/d\tau = (u^t, 0, 0, 0) = (e^{-\Phi(r)}, 0, 0, 0)$. The observer's four-acceleration is $a^\mu = u^\mu{}_{;\nu}\,u^\nu$, so that taking into account metric (17), we have $a^t = 0$ and

$$a^r = \Gamma^r{}_{tt}\left(\frac{dt}{d\tau}\right)^2 = \Phi_{,r}\,(1 - b/r)\,. \tag{18}$$

Note that from the geodesic equation, a radially moving test particle, which initially starts at rest, obeys the following equation of motion

$$\frac{d^2r}{d\tau^2} = -\Gamma^r{}_{tt}\left(\frac{dt}{d\tau}\right)^2 = -a^r\,. \tag{19}$$

a^r is the radial component of proper acceleration that an observer must maintain in order to remain at rest at constant r, θ, ϕ. One may consider that the geometry is attractive if $a^r > 0$, i.e., observers must maintain an outward-directed radial acceleration to keep from being pulled into the wormhole; and repulsive if $a^r < 0$, i.e., observers must maintain an inward-directed radial acceleration to avoid being pushed away from the wormhole. This distinction depends on the sign of $\Phi_{,r}$, as is transparent from Eq. (18). In particular, for a constant redshift function, $\Phi_{,r}(r) = 0$, static observers are also geodesic. Thus, the convention used is that $\Phi_{,r}(r)$ is positive for an inwardly gravitational attraction, and negative for an outward gravitational repulsion.

The above analysis is of particular interest for particles moving in circular orbits around wormholes, which are unstable for the specific case of $\Phi_{,r}(r) < 0$, due to the outward gravitational repulsion. Therefore, we only consider the case of $\Phi_{,r}(r) > 0$, and in particular the example of

$$\Phi(r) = -\frac{r_0}{r} \tag{20}$$

is considered throughout this work.

The effective potential, given by Eq. (13), which determines the geodesic motion of the test particles in the equatorial plane of the metric given by Eq. (17), is rewritten here for convenience

$$V_{eff}(r) \equiv e^{2\Phi}\left(1 + \frac{\widetilde{L}^{\,2}}{r^2}\right)\,. \tag{21}$$

The specific case of $\Phi(r) = -r_0/r$ is depicted in Fig. 1, for a wormhole with a total mass of $M = 0.06776 M_\odot$ or $r_0 = GM/c^2 = 10^4$cm, and for particles orbiting with the specific angular momentum of $\widetilde{L} = 4M$. The effective potential of the Schwarzschild geometry, depicted as the solid line, is plotted for comparison.

In Fig. 1, we also compare the angular velocity Ω, the specific energy $\widetilde{E}$ and the specific angular momentum $\widetilde{L}$ of the orbiting particles for the two types of the potential. Since these quantities, given by Eqs. (14)-(16), depend only on the metric function $\Phi(r)$, they are identical for each wormhole geometry, independently of the choice of the shape function $b(r)$. The only quantity in the flux integral (7) which has a dependence of $b(r)$ is the metric determinant. For the invariant volume element of the various types of wormholes we have

$$\sqrt{-g} = \frac{r^2 e^{\Phi}}{\sqrt{1 - b(r)/r}}\,, \tag{22}$$

which can give different flux values in computing Eq. (7) for different choices of $b(r)$. As seen in Fig. 1, for the wormhole geometry under study the orbiting particles gain somewhat less angular velocity, specific energy and specific angular momentum than in the Schwarzschild potential.

In Figs. 2–4, we plot the energy flux, the disk temperature and the emission spectra $\omega L(\omega)$ emitted by the accretion disk with a mass accretion rate of $\dot{M}_0 = 10^{-12} M_\odot/\mathrm{yr}$ for various wormhole geometries. In particular, in the left plots, of the respective figures, we have used the following shape functions:

$$b(r) = r_0\,, \qquad b(r) = \frac{r_0^2}{r}\,, \qquad b(r) = \sqrt{r r_0}\,, \tag{23}$$

and in the right plot, the shape function

$$b(r) = r_0 + \gamma r_0\left(1 - \frac{r_0}{r}\right)\,, \tag{24}$$

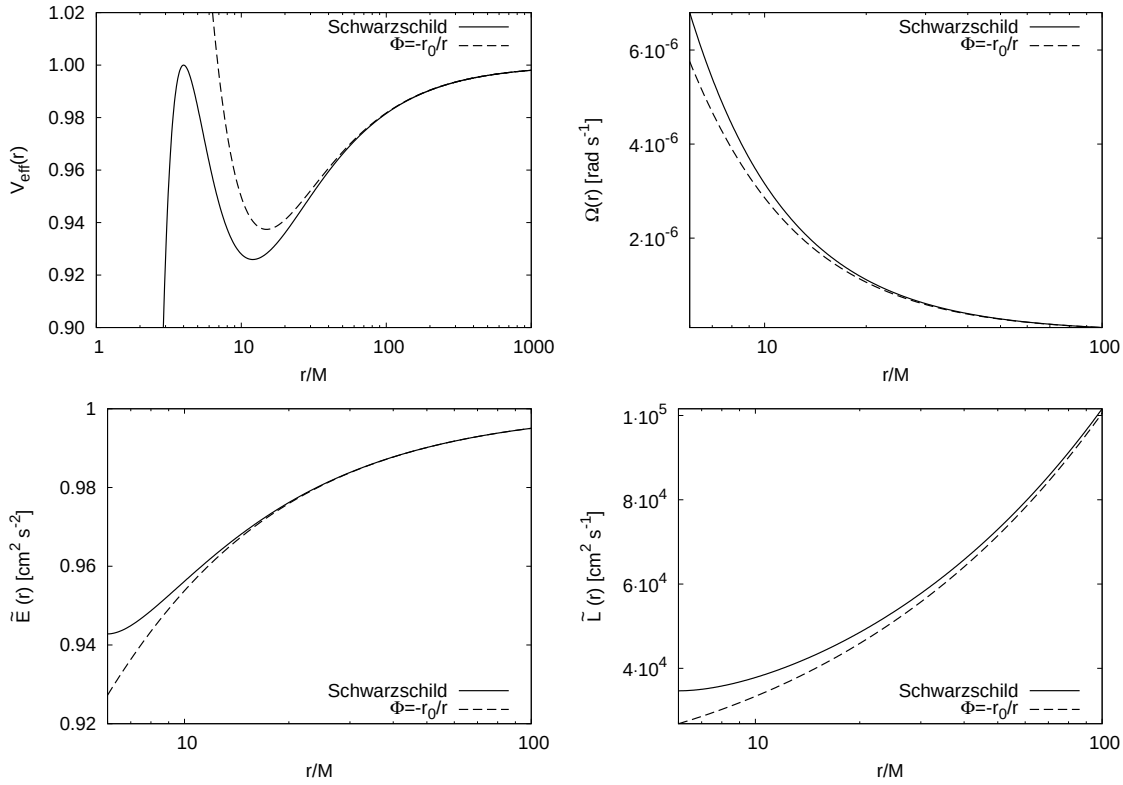

FIG. 1: The effective potential $V_{eff}(r)$ (top left hand), the angular velocity Ω (top right hand), the specific energy $\widetilde{E}$ (bottom left hand) and the specific angular momentum $\widetilde{L}$ (bottom right hand) of the orbiting particles for a wormhole of a total mass $M = 0.06776M_{\odot}$ and for the specific angular momentum $\widetilde{L} = 4M$. The specific case of $\Phi = -r_0/r$ is considered, and is compared with the Schwarzschild solution, which is depicted as the solid line.

has been used, with $0 < \gamma < 1$. Note that not only Ω $\widetilde{E}$ and $\widetilde{L}$ have smaller values for the wormhole geometry under study than in the case of static black holes but the invariant volume element (22) also takes rather small values for any choice of the function $b(r)$. Consequently more energy is radiated away than in the Schwarzschild potential, which is reflected in Fig. 2.

The marginally stable orbit is located at the radius $2r_0$ for the wormholes, whereas we have $r_{ms} = 6r_0$ for the Schwarzschild black hole. As a result, the inner edge of the disk is closer to the throat of the wormhole than to the event horizon of the black hole, comparing any wormhole and black hole with the same geometrical mass r_0. The wormhole efficiency ϵ of the conversion of the accreted mass into radiation is 0.1422 which is much higher than $\epsilon = 0.0572$ for the black hole. Although 14% is still less than the 40% obtained for Kerr black holes, it demonstrates that static wormholes provide a more efficient accretion mechanism to convert the gravitational energy into disk luminosity than the mass accretion driven by static black holes.

These effects in the disk radiation can also be observed in the radial profiles of temperature corresponding to the flux distributions, shown in Fig. 3, and in the emission spectrum $\omega L(\omega)$ of the accretion disks, which are plotted in Fig. 4.

Thus, for the static and spherically symmetric solutions, we conclude that the specific signatures, that appear in the electromagnetic spectrum, lead to the possibility of distinguishing wormhole geometries from the Schwarzschild solution by using astrophysical observations of the emission spectra from accretion disks.

IV. DISCUSSIONS AND FINAL REMARKS

In the present paper, we have studied thin accretion disk models applied to the study of static and spherically symmetric wormhole geometries, and have carried out an analysis of the properties of the radiation emerging from the surface of the disk. In classical general relativity, wormholes are supported by exotic matter, which involves a stress energy tensor that violates the null energy condition. Thus, it has proved interesting to analyze the properties, namely, the time averaged energy flux, the disk temperature and the emission spectra of the accretion disks around these wormholes comprising of exotic matter. For the static and spherically symmetric wormhole geometries under study, we have verified that the potential well is higher than the Schwarzschild potential,

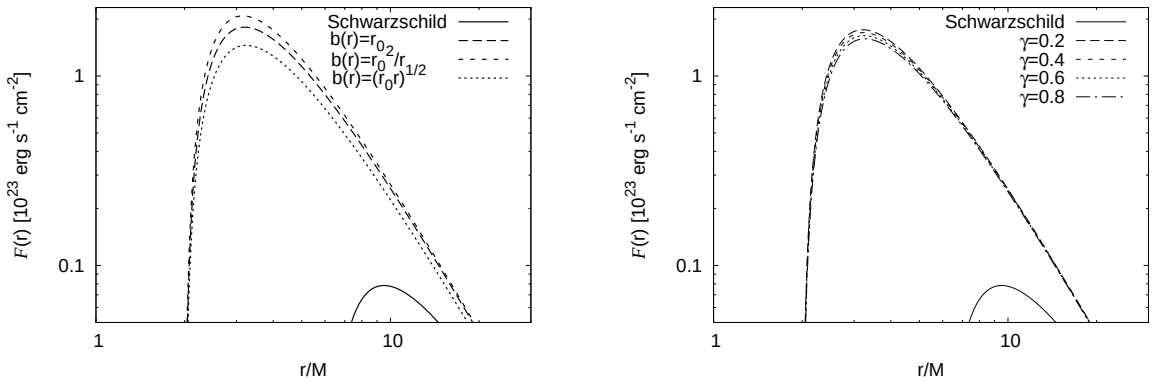

FIG. 2: The time averaged flux $\mathcal{F}(r)$ radiated by the disk for a wormhole of an effective mass $M = 0.06776M_{\odot}$ and a mass accretion rate $\dot{M}_0 = 10^{-12}M_{\odot}/\mathrm{yr}$. Different shape functions were evaluated, namely, in the left plot the cases chosen were: $b(r) = r_0$ (the long dashed line), $b(r) = r_0^2/r$ (the short dashed line) and $b(r) = (r_0 r)^{1/2}$ (the dotted line), respectively. The flux emitted by a disk around a Schwarzschild black hole is plotted with a solid line. The right plot depicts the case of $b(r) = r_0 + \gamma r_0(1 - r_0/r)$, with varying values of γ.

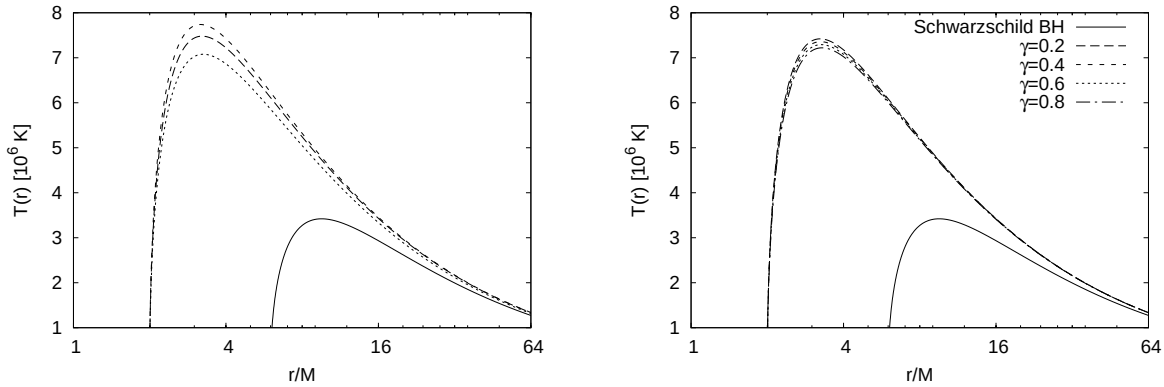

FIG. 3: Temperature distribution of the accretion disk for a wormhole of an effective mass $M = 0.06776M_{\odot}$ and a mass accretion rate $\dot{M}_0 = 10^{-12}M_{\odot}/\mathrm{yr}$. Different shape functions were evaluated, namely, in the left plot the chosen cases were: $b(r) = r_0$ (the long dashed line), $b(r) = r_0^2/r$ (the short dashed line) and $b(r) = (r_0 r)^{1/2}$ (the dotted line), respectively. The disk temperature profile for a Schwarzschild black hole is plotted with a solid line. The right plot depicts the case of $b(r) = r_0 + \gamma r_0(1 - r_0/r)$, with varying values of γ.

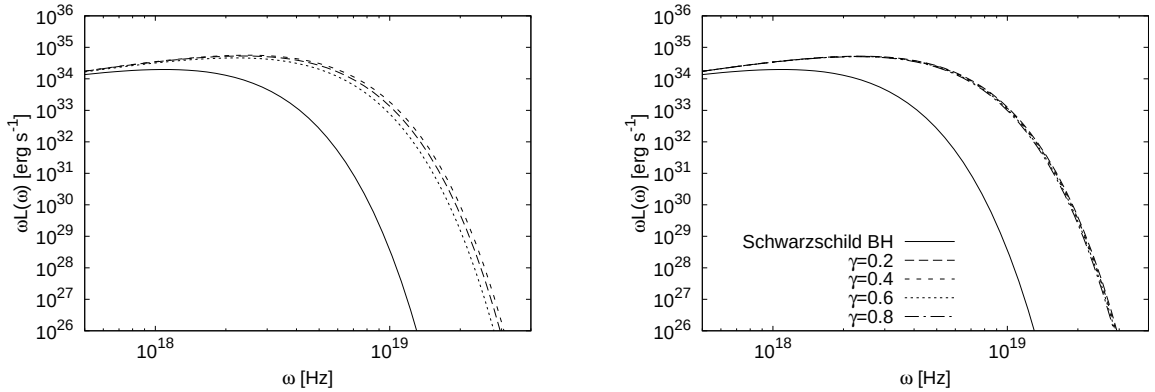

FIG. 4: The emission spectra $\omega L(\omega)$ of the accretion disks for a wormhole of effective mass $M = 0.06776M_{\odot}$ and a mass accretion rate of $\dot{M}_0 = 10^{-12}M_{\odot}/\mathrm{yr}$. Different shape functions were evaluated, namely, in the left plot the chosen cases were: $b(r) = r_0$ (the long dashed line), $b(r) = r_0^2/r$ (the short dashed line) and $b(r) = (r_0 r)^{1/2}$ (the dotted line), respectively. The flux emitted by a disk around a Schwarzschild black hole is plotted with a solid line. The right plot depicts the case of $b(r) = r_0 + \gamma r_0(1 - r_0/r)$, with varying values of γ.

and consequently more energy is radiated away. These effects in the disk radiation were also observed in the radial profiles of temperature corresponding to the flux distributions, and in the emission spectrum $\omega L(\omega)$ of the accretion disks. Thus, for these solutions, we conclude that the specific signatures, that appear in the electromagnetic spectrum, lead to the possibility of distinguishing wormhole geometries from the Schwarzschild solution by using astrophysical observations of the emission spectra from accretion disks.

In this context, observations in the near-infrared (NIR) or X-ray bands have provided important information about the spin of the black holes, or the absence of a surface in stellar type black hole candidates. In the case of the source Sgr A*, where the putative thermal emission due to the small accretion rate peaks in the near infrared, the results are particularly robust. However, up to now, these results have confirmed the predictions of general relativity mainly in a qualitative way, and the observational precision achieved cannot distinguish between the different classes of compact/exotic objects that appear in the theoretical framework of general relativity [9]. However, important technological developments may allow to image black holes and other compact objects directly [25]. A background illuminated black hole will appear in a silhouette with radius $\sqrt{27}GM/c^2$, with an angular size of roughly twice that of the horizon, and may be directly observed. With an expected resolution of 20 μas, submillimeter very-long baseline interferometry (VLBI) would be able to image the silhouette cast upon the accretion flow of Sgr A*, with an angular size of ~ 50 μas, or M87, with an angular size of ~ 25 μas. For a black hole embedded in an accretion flow, the silhouette will generally be asymmetric regardless of the spin of the black hole. Even in an optically thin accretion flow an asymmetry will result from special relativistic effects (aberration and Doppler shifting). In principle, detailed measurements of the size and shape of the silhouette could yield information about the mass and spin of the central black hole, and provide invaluable information on the nature of the accretion flows in low luminosity galactic nuclei.

We suggest that by using the same imaging technique, which gives the physical/geometrical properties of the silhouette of the compact object cast upon the accretion flows on the compact objects, would be able to provide clear observational evidence for the existence of wormholes, and differentiate them from other types of compact general relativistic objects. We conclude by pointing out that specific signatures appear in the electromagnetic spectrum of the thin accretion disks around wormholes, thus leading to the possibility of detecting and distinguishing wormhole geometries by using astrophysical observations of the emission spectra from accretion disks. It is also interesting to generalize the analysis carried out in this work to stationary and axially symmetric wormhole spacetimes, and compare the emission spectra to the Kerr solution. Work along these lines is currently underway.

Acknowledgments

The work of TH is supported by an RGC grant of the government of the Hong Kong SAR. ZK was supported by the Hungarian Scientific Research Fund (OTKA) grant no.69036. FSNL was funded by Fundação para a Ciência e a Tecnologia (FCT)–Portugal through the grant SFRH/BPD/26269/2006.

[1] C. M. Urry and P. Padovani, Publ. Astron. Soc. of the Pacific **107**, 803 (1995).
[2] M. Miyoshi, J. Moran, J. Herrnstein, L. Greenhill, N. Nakai, P. Diamond and M. Inoue, Nature **373**, 127 (1995).
[3] I. D. Novikov and K. S. Thorne, in Black Holes, ed. C. DeWitt and B. DeWitt, New York: Gordon and Breach (1973).
[4] N. I. Shakura and R. A. Sunyaev, Astron. Astrophys. **24**, 33 (1973).
[5] D. N. Page and K. S. Thorne, Astrophys. J. **191**, 499 (1974).
[6] K. S. Thorne, Astrophys. J. **191**, 507 (1974).
[7] S. Bhattacharyya, A. V. Thampan and I. Bombaci, Astron. Astrophys. **372**, 925 (2001).
[8] D. Torres, Nucl. Phys. B **626**, 377 (2002).
[9] Y. F. Yuan, R. Narayan and M. J. Rees Astrophys. J. **606**, 1112 (2004).
[10] F. S. Guzman, Phys. Rev. D **73**, 021501 (2006).
[11] C. S. J. Pun, Z. Kovacs and T. Harko, Phys. Rev. D **78**, 024043 (2008).
[12] M. S. Morris and K. S. Thorne, Am. J. Phys. **56**, 395 (1988).
[13] H. G. Ellis, J. Math. Phys. **14** (1973) 104; K. A. Bronnikov, Acta Phys. Polon. B **4** (1973) 251.
[14] G. Clement, Gen. Rel. Grav. **16**, 131 (1984); G. Clement, Gen. Rel. Grav. **16**, 477 (1984); G. Clement, Gen. Rel. Grav. **16**, 491 (1984).
[15] B. Bhawal and S. Kar, Phys. Rev. D **46**, 2464-2468 (1992); G. Dotti, J. Oliva, and R. Troncoso, Phys. Rev. D **75**, 024002 (2007).
[16] L. A. Anchordoqui and S. E. P Bergliaffa, Phys. Rev. D **62**, 067502 (2000); K. A. Bronnikov and S.-W. Kim, Phys. Rev. D **67**, 064027 (2003); M. La Camera, Phys. Lett. **B573**, 27-32 (2003); F. S. N. Lobo, Phys. Rev. D **75**, 064027 (2007).
[17] K. K. Nandi, B. Bhattacharjee, S. M. K. Alam and J. Evans, Phys. Rev. D **57**, 823 (1998).
[18] R. Garattini and F. S. N. Lobo, Class. Quant. Grav. **24**, 2401 (2007).
[19] C. G. Boehmer, T. Harko and F. S. N. Lobo, Phys. Rev. D **76**, 084014 (2007); C. G. Boehmer, T. Harko and F. S. N. Lobo, Class. Quant. Grav. **25**, 075016 (2008).
[20] S. Sushkov, Phys. Rev. D **71**, 043520 (2005);

F. S. N. Lobo, Phys. Rev. D **71**, 084011 (2005); F. S. N. Lobo, Phys. Rev. D **71**, 124022 (2005); F. S. N. Lobo, Phys. Rev. D **73**, 064028 (2006).
[21] F. S. N. Lobo, Class. Quant. Grav. **25**, 175006 (2008).
[22] J. P. S. Lemos, F. S. N. Lobo and S. Quinet de Oliveira, Phys. Rev. D **68**, 064004 (2003).
[23] F. S. N. Lobo, arXiv:0710.4474 [gr-qc].
[24] F. S. N. Lobo, Phys. Rev. D **75**, 024023 (2007).
[25] A. E. Broderick and R. Narayan, Astrophys. JL. **636**, L109 (2006).